Accepted Manuscript

Towards efficient oxygen reduction reaction electrocatalysts through graphene doping

Diana M. Fernandes, Penny Mathumba, António J.S. Fernandes, Emmanuel I. Iwuoha, Cristina Freire

PII: S0013-4686(19)31318-0

DOI: https://doi.org/10.1016/j.electacta.2019.06.175

Reference: EA 34482

To appear in: *Electrochimica Acta*

Received Date: 18 February 2019

Revised Date: 27 June 2019

Accepted Date: 28 June 2019

Please cite this article as: D.M. Fernandes, P. Mathumba, Antó.J.S. Fernandes, E.I. Iwuoha, C. Freire, Towards efficient oxygen reduction reaction electrocatalysts through graphene doping, *Electrochimica Acta* (2019), doi: https://doi.org/10.1016/j.electacta.2019.06.175.

TOWARDS EFFICIENT OXYGEN REDUCTION REACTION ELECTROCATALYSTS THROUGH GRAPHENE DOPING

Diana M. Fernandes[a*], Penny Mathumba[b], António J. S. Fernandes[c], Emmanuel I. Iwuoha[b], Cristina Freire[a]

[a] REQUIMTE-LAQV/Departamento de Química e Bioquímica, Faculdade de Ciências, Universidade do Porto, 4169-007 Porto, Portugal.

[b] Department of Chemistry, Faculty of Science University of the Western Cape (UWC), Cape Town, South Africa

[c] Instituto de Nanoestruturas, Nanomodelação e Nanofabricação (I3N), Departamento de Física, Universidade de Aveiro, Campus Universitário de Santiago, 3810-193 Aveiro, Portugal.

*Corresponding authors: Dr. Diana M. Fernandes (diana.fernandes@fc.up.pt)

Keywords: Oxygen reduction reaction; Graphene flakes; N, S-doping; metal oxides; fuel cells

Abstract

The incessant and drastic growth of global energy demand make it imperative to develop new affordable high-quality materials at a large scale to act as powerful electrocatalysts (ECs) on the relevant energy reactions.

Here, we report the synthesis and characterization (FTIR, Raman, XPS, XRD, TEM and SEM) of new engineered electrocatalysts based on situ co-precipitation of Co_3O_4 or Mn_3O_4 nanoparticles in the presence of N, S-doped graphene (Co/N_3S_3-GF and Mn/N_3S_3-GF). The nitrogen, sulphur dual-doped graphene was achieved by a scalable dry ball-milling procedure followed by thermal treatment using graphene flakes as carbon source and trithiocyanuric acid as the precursor.

The three materials prepared were applied as electrocatalysts for the oxygen reduction reaction (ORR) and demonstrated excellent electrocatalytic performance in alkaline medium with Co/N_3S_3-GF and Mn/N_3S_3-GF presenting onset potentials of 0.87 V vs. RHE. These were comparable to Pt/C onset potential (0.91 V). All materials showed good diffusion-limiting current densities (-3.49 – -4.17 mA cm^{-2}) and selectivity for the 4-electron O_2 reduction to H_2O. Furthermore, the Co/N_3S_3-GF and Mn/N_3S_3-GF electrocatalysts presented good tolerance to methanol poisoning and good stability with current retentions (76 – 81%).

The approach followed in this work showed that affordable, simple and scalable procedures can be applied to develop ORR electrocatalysts with enhanced performances.

1. Introduction

The current high demand of energy has led to a continuous and rapid increase of the depletion rate of fossil fuel reserves.[1, 2] Additionally, the combustion of fossil fuels is one of the major causes of emission of dangerous gases to the atmosphere, which leads to several environmental adverse effects. The incessant increase of their cost and the inherent environmental issues have led to an urgent development of eco-friendly sustainable alternative energy sources and energy conversion devices. Among these are metal-air batteries and fuel cells. However, their commercialization is hindered owing to the high cost of various fuel cell components.[2] Also, one of the major cornerstones of these systems is the oxygen reduction reaction (ORR) that occurs at the cathode and normally has sluggish kinetics.[3]

Platinum and Platinum-based ECs are still considered the most efficient ECs for ORR by introducing lower energy intermediates. However, the low availability of Pt, that increases dramatically its price, is responsible for the limited use of Pt-based FCs. Platinum ECs also face severe problems in terms of tolerance to methanol crossover and stability under operating conditions.[4] As a consequence, intensive research efforts have been devoted to the development of alternative ECs based on more abundant and cost-effective elements without compromising the electrocatalytic activity.[4-6]

Transition metal oxides, in particular cobalt and manganese oxides, constitute a auspicious class of non-precious metal ECs for ORR due to the intrinsic electrocatalytic activity ascribed to their inherent mixed-valence state and low environmental impact.[5, 7-10] Still, the low electrical conductivity of these metal oxides limits their performance as electrode materials and this has prompted researchers to immobilize them onto different electrically conductive materials in order to overcome this drawback.

Several carbon-based supports have been used for this propose as graphene,[7, 11, 12] graphene oxide,[13]carbon nanotubes[14] and respective doped carbon materials.[15-17] The

choice of a good support can afford additional anchoring positions where the ECs can be attached. Amongst the existing carbon-based materials, one has proved itself as an outstanding support – graphene. This is due its known high surface area, excellent electrical conductivity and good chemical/mechanical stability.[11, 18] Through doping with different heteroatoms like nitrogen, boron, sulphur or phosphorous, the electronic properties of pristine graphene can be tuned giving rise to increased performances.[19-21] Doping modifies the atomic scale structures and the charge distribution of the carbon atoms is disturbed which generates active sites on graphene that can act as anchoring sites to attach other species.[19, 22]

In this work, we explore the nitrogen/sulphur (N, S) dual-doped graphene flakes as a support. Two nanocomposites of Co_3O_4 and Mn_3O_4 nanoparticles supported on the nitrogen/sulphur (N, S) dual-doped graphene flakes (Co/N_3S_3-GF and Mn/N_3S_3-GF) have been designed and applied as ORR electrocatalysts. The N, S dual-doped graphene was prepared by a simple and scalable procedure using trithiocyanuric acid as the nitrogen and sulphur. Some reports can be found in literature regarding the use of trithiocyanuric acid as precursor for the CNTs co-doping[23] or in the preparation of carbonaceous materials together with other precursors such as melamine.[24, 25] As far as we know, this is the first time this material is used as precursor for the preparation of dual-doped graphene flakes.

The nanocomposites benefited from the covalent coupling effect between metal oxide nanoparticles and dual-doped graphene flakes exhibiting superior ORR electrocatalytic activities.

2. Experimental Section

2.1.Materials and characterization methods

Graphene flakes (Graphene Technologies, Lot GTX-7/6−10.4.13), 1,3,5-Triazine-2,4,6-trithiol (Trithiocyanuric acid, N_3S_3, Sigma-Aldrich), manganese (II) chloride tetrahydrate ($MnCl_2 \cdot 4H_2O$, Merck), cobalt (II) chloride hexahydrate ($CoCl_2$, Fluka), 1-amino-2-propanol (MIPA, 93%, Aldrich) and absolute ethanol (Fisher Scientific) were used in the materials preparation and were used as received.

For the electrochemical studies, the following reagents and solvents were used: potassium hydroxide (KOH, 99.99 %, Sigma-Aldrich), platinum nominally 20 % on carbon black (Pt/C 20 wt%, HiSPEC® 3000, Alfa Aesar), Nafion (5 wt.% in lower aliphatic alcohols and water, Aldrich), isopropanol (99.5 %, Aldrich), methanol (anhydrous, VWR) and hydrogen peroxide solution (30 wt.% in water, ACS reagent, Sigma Aldrich). Ultrapure water (18.2 MΩ cm at 25ºC, Millipore) was used throughout the experiments.

For the synthesis of S, N-doped graphene flakes a MM200 Retsch mixer mill using zirconium oxide grinding jars (25 mL) and zirconium oxide balls (2 mm each ball, ≈ 100 balls) was used.

All prepared materials were characterized by several techniques such as FTIR, Raman, XPS, XRD, TEM and SEM. All details (apparatus and methods) regarding these can be found in the supporting information (SI) file.

2.2.Materials preparation

For the synthesis of S, N-doped graphene flakes, commercial graphene flakes (400 mg) were mixed with N_3S_3 and subjected to ball milling for 5 h at a constant vibrational frequency of 15 Hz. The resulting powder calcined at 800 °C under nitrogen flow for 1 h and N_3S_3-GF was obtained.

The Co_3O_4 nanoparticles were prepared through a co-precipitation procedure where a 3.0 mol dm^{-3} solution of MIPA was added to 50 mL of an aqueous solution of $CoCl_2 \cdot 6H_2O$

(5.0 mmol), at a rate of 50 mL h^{-1}, until *pH* = 10 was reached. The reaction mixture was stirred for 24 h, at room temperature. The resulting material was filtered, thoroughly washed with water and ethanol, and dried under vacuum. Then, the powder was calcined under air, at 250 ºC for 3 h. The Mn_3O_4 nanoparticles were prepared through a similar procedure: MIPA was added to 100 mL of an aqueous solution of $MnCl_2 \cdot 4H_2O$ (11.0 mmol), until *pH* = 10 and the mixture was stirred for 24 h at 80 ºC under reflux. The calcination was performed under air, at 300 ºC for 5 h.

The Co/N_3S_3-GF and Mn/N_3S_3-GF nanocomposites were prepared by Co_3O_4 or Mn_3O_4 in situ co-precipitation in the presence of S, N-GF. Briefly, N_3S_3-GF (235 or 217 mg) were dispersed in 50 mL of an aqueous solution containing $CoCl_2.6H_2O$ (4 mmol) or $MnCl_2 \cdot 4H_2O$ (4.4 mmol) and the same procedure as those described for pure Co_3O_4 or Mn_3O_4 nanoparticles were adopted.

2.3.ORR electrochemical performance

For the cyclic (CV) and linear weep voltammetry (LSV) experiments was used a potentiostat/galvanostat Autolab PGSTAT 302N (EcoChimie B.V.), controlled by the NOVA v2.0 software. The working electrode was a modified glassy carbon rotating disk electrode, RDE (Metrohm, 3 mm of diameter) while as reference and counter electrodes were used an Ag/AgCl (Metrohm, 3 mol dm^{-3} KCl) and a carbon rod (Metrohm, 2 mm of diameter), respectively.

Prior to modification, the electrode was cleaned by already reported procedure (see SI file for more details).[26]The RDE was then modified through the deposition of a 5 μL drop of the selected ECs dispersion onto its surface and allowing it to dry under a flux of air. The ECs dispersion was prepared as follows: 1 mg of selected material or Pt/C were mixed with 2-

propanol/water/Nafion solvent mixture (125/125/20 μL) and dispersed using an ultrasonic bath for 15 min.

All the electrochemical experiments were carried out in N_2- or O_2-saturated 0.1 mol dm^{-3} KOH electrolyte through the purge of the electrolyte for at least 30 min with the selected gas. Both the CV and LSV measurements were performed between E_p = 0.26 and 1.46 V vs. RHE at 0.005 V s^{-1}. Additionally, rotation speeds in the range 400 - 3000 rpm were used for the LSV experiments. For the chronoamperometry (CA) tests a rotation speed of 1600 rpm for 20 000 s at a potential = 0.5 V vs. RHE was used. Tolerance to methanol was assessed by CA at E = 0.5 V vs. RHE and 1600 rpm for 2000 s.

The effective ORR current, and other important ORR parameters like onset potentials (E_{onset}), diffusion-limiting currents (j_L), Tafel slopes and the number of electrons transferred per O_2 molecule (n_{O2}) were determined as described elsewhere[26] (see SI file for more detailed information).

Rotating ring disk electrode (RRDE) measurements in O_2-saturated KOH solution were also performed in order to obtain a more in-depth insight of the ORR electrocatalytic activity of the ECs. The H_2O_2 yields were determined from the ring and disk currents (IR and ID, respectively), and the current collection efficiency of the Pt ring (N = 0.25, in this case) using Eq. 1:[27]

$$\% H_2O_2 = 200 \times \frac{i_R / N}{i_D + i_R / N} \qquad \text{(Eq. 1)}$$

3. Results and Discussion

3.1. Materials preparation and characterization

The FTIR spectra of the Co_3O_4 and Mn_3O_4 nanoparticles and the corresponding Co/N_3S_3-GF and Mn/N_3S_3-GF nanocomposites are shown in Figure 1, while those for GF and N_3S_3-GF are presented in Figure S1 in the supporting information (SI). The FTIR

characterization of GF was previously reported[26] and the spectrum presented several weak vibration bands. Those at 3440, 1631, 2853 and 2921 cm^{-1} correspond to the stretching vibrations of OH groups, C=O and aromatic sp^2 C–H, respectively. The other at 1581, 1378 and 1140 cm^{-1} are attributed to C=C stretching vibrations, vibration of hydroxyls groups and C−O stretching vibration, respectively.[26] The N_3S_3-GF spectrum presents five bands at 3437, 1637, 1580, 1382 and 1191 cm^{-1}. The band at 3437 cm^{-1} is assigned to OH stretching vibrations, that at 1580 to C=C stretching vibrations and the one at 1191 cm^{-1} to C−O stretching vibration. The other two (1637 and 1382 cm^{-1}) are assigned to C=N and C−N stretching vibrations, respectively.[26] The FTIR spectra of Co/N_3S_3-GF (Figure 1 (a)) confirms the presence of the Co_3O_4 NPs on the final nanocomposite as both spectra present two sharp bands at 566 and 666 cm^{-1} attributed to Co(III) Co–O stretching modes at octahedral position and Co(II) at tetrahedral position in the spinel oxide structure, respectively. Other two bands are observed at 1634 and 3418 cm^{-1} and are assigned to the O–H bending and stretching vibration modes from adsorbed molecules of water and MIPA.[28] The bands corresponding to the carbon material are also observed between 946 and 1532 cm^{-1}. The FTIR spectra of Mn_3O_4 NPs and Mn/N_3S_3-GF are depicted in Figure 1 (b) and two intense vibrational bands are observed for both compounds at 514 and 621 cm^{-1} which are assigned to the distortion vibration of Mn–O in octahedral sites and Mn–O stretching vibration mode in tetrahedral sites, respectively.[29] The band observed at ≈ 422 cm^{-1} is assigned to the vibration of Mn^{3+}-O in octahedral sites.[30] Additionally, the band at ≈ 1166 cm^{-1} can be attributed to the vibration mode of hydroxyl group of the nanoparticles capping agent MIPA while that at ≈ 1631 cm^{-1} to O–H bending from MIPA and adsorbed water molecules on the surface of the nanoparticles.[28] As for the Co/N_3S_3-GF, the bands corresponding to the carbon material are also observed.

(Insert Figure 1)

Figure 2 shows the Raman spectra of N_3S_3-GF, Co_3O_4 and Mn_3O_4 nanoparticles, and the corresponding nanocomposites (Co/N_3S_3-GF and Mn/N_3S_3-GF). The Raman spectrum of N_3S_3-GF shows an intense peak at 1575 cm^{-1} which is assigned to the first order scattering of the E_{2g} mode, another at 1343 cm^{-1} attributed to the D mode that is induced by the structural disorder and one at 2680 cm^{-1} ascribed to the 2D mode.[31] For the Co_3O_4 nanoparticles (Figure 2 (a)), one sharp and intense peak is observed at 668 cm^{-1} and other three peaks at 603, 503 and 461 cm^{-1} which are attributed to the A_{1g}, F_{2g}, F_{2g} and E_g Raman active modes of Co_3O_4 structure, respectively. The nanocomposite Co/N_3S_3-GF exhibited the peaks corresponding to both the carbon materials (1349, 1573 and 2689 cm^{-1}) and the Co_3O_4 NPs (665, 600, 507 and 465 cm^{-1}) confirming its successful preparation. For the Mn_3O_4 nanoparticles (Figure 2 (b)) are observed three peaks: one intense and sharp peak at 638 cm^{-1}, characteristic of the vibration of oxygen atoms inside the octahedral MnO_6 unit, and two less intense at 345 and 286 cm^{-1}. These peaks are assigned to the A_{1g}, T_{2g} and E_g Raman active modes of the spinel Mn_3O_4 structure.[29, 32, 33] The nanocomposite Mn/N_3S_3-GF, in addition to the presence of these peaks (at 640, 356 and 273 cm^{-1}), which confirms the in situ synthesis of the Mn_3O_4 NPs, it is possible to observe the peaks corresponding to the D, G and 2D modes of the carbon material (1342, 1572 and 2683 cm^{-1}). The shifts in all the Raman bands confirm the interaction between the Co_3O_4 and Mn_3O_4 nanoparticles with the N_3S_3-GF.

(Insert Figure 2)

Figure 3 shows the XRD patterns of both nanocomposites prepared (Co/N_3S_3-GF (a) and Mn/N_3S_3-GF (b)) and of the corresponding pure nanoparticles. For the Co_3O_4 nanoparticles (Figure 3 (a)), the diffraction peaks observed at 2θ of 19°, 31°, 37°, 38°, 45°, 59° and 65° are indexed to the planes (111), (220), (311), (222), (400), (511) and (440) of

face-centered-cubic phase of Co_3O_4 spinel structure, with Co^{II} and Co^{III} ions in a 1:2 proportion ($Co^{II}Co^{III}{}_2O_4$) and where the Co^{II} ions are occupying the tetrahedral sites while the Co^{III} the octahedral sites.[34, 35] The XRD patterns of Co/N_3S_3-GF nanocomposite presents, besides the peaks assigned to Co_3O_4 NPs, one diffraction peak at 2θ = 26º corresponding to the (002) planes of stacked graphene layers from the doped graphene (N_3S_3-GF). The XRD patterns of Mn_3O_4 NPs (Figure 3 (b)) presents the diffraction peaks at 2θ of 18º (101), 29º (112), 31º (200), 32º (103), 36º (211), 38º (004), 44º (220), 51º (105), 54º (312), 56º (303), 58º (321) and 60º (224). These peaks are indexed to the Mn_3O_4 spinel structure which contains the Mn^{II} and Mn^{III} ions in the same proportion as the above described for the Co_3O_4 NPs.[29] The XRD patterns of Mn/N_3S_3-GF nanocomposite presents the diffraction peaks corresponding to the Mn_3O_4 NPs and also that at 2θ = 26º attributed previously to the N_3S_3-GF. These results corroborate the Raman results and confirm the synthesis of nanoparticles *in situ* onto the N_3S_3-GF.

(Insert Figure 3)

The surface composition of N_3S_3-GF, Co/N_3S_3-GF and Mn/N_3S_3-GF was assessed by XPS and the surface atomic % are summarised in Table 1. The data previously obtained for GF[26] was also included for comparison. The C 1s high-resolution spectrum of the pristine graphene flakes (Figure S2 (a), SI) was already reported and was fitted with five peaks at: 284.6 eV (sp^2, C-C, C=C), 286.2 eV (C-O), 287.1 eV (C=O), 288.1 eV (O-C=O), and 290.6 eV (π-π* transition).[26] Figure 4 and S3 and S4 (a) show the C 1s high-resolution spectra of Co/N_3S_3-GF, N_3S_3-GF and Mn/N_3S_3-GF, respectively. The fitting of these was similar to that of GF. The main differences were the presence of a new small peak at ≈ 283.3 eV attributed to the C-S-C[36] (from doping with N_3S_3) and that the peak at approximately 286 eV has also the contribution from C-N bonds due to the GF doping with nitrogen (N_3S_3).[26]

The O 1s high-resolution spectra of GF and N_3S_3-GF are shown in Figures S2 (a) and S3 (a), respectively and were fitted with three peaks: one at ≈ 531 eV corresponding to C=O, one at ≈ 532 eV attributed to C-O and another at ≈ 533 eV assigned to O-C=O.[26, 37] For the nanocomposites Co/N_3S_3-GF (Figure 4 (b)) and Mn/N_3S_3-GF (Figure S4 (b)) the O 1s spectra were deconvoluted into five peaks at: 529.7 eV attributed to O^{2-} in crystal lattices of Co_3O_4 and Mn_3O_4, ≈ 531 eV assigned to adsorbed hydroxyl groups onto the Co_3O_4/Mn_3O_4 structures, ≈ 531.5 eV corresponding to the contribution of O-C (phenol, epoxy) and O=C (ketones, quinones, aldehydes) from N_3S_3-GF, ≈ 532.2 eV attributed to hydroxyl groups from MIPA and finally ≈ 533.5 eV assigned to water molecules from Co_3O_4/Mn_3O_4 structures.[38, 39] The N 1s XPS spectrum of N_3S_3-GF (Figure S3 (c)) was fitted with three main peaks at 398.1, 399.5 and 400.6 eV attributed to pyridinic-N, pyrrolic-N, and graphitic N, respectively. Those at 399.5 and 400.6 eV may be attributed to the π-conjugated system with a pair of p-electrons in graphene layers while that at 400.6 eV demonstrates the replacement of N atoms in the carbon layers.[20, 40, 41] The spectra for the nanocomposites are similar and are given in Figures 4 (c) and S4 (c). In Table S1 can be observed the core-level binding energies extracted from the XPS high resolution N 1s spectra for all as-prepared materials and the relative atomic percentages of each type of nitrogen. The S 2p XPS spectra are somewhat complex due to spin-orbital coupling phenomenon. Figure S3 (c) shows the spectra of N_3S_3-GF while those of Co/N_3S_3-GF and Mn/N_3S_3-GF are depicted in Figures 4 (d) and S4 (d), respectively. The pair of peaks at ≈ 163.8 eV ($2p_{3/2}$) and 164.9 eV ($2p_{1/2}$) can be attributed to the C-S-C covalent bonds, the ones between 165 and 166.5 eV to C-SH and those between 168 and 169.5 eV attributed to some oxidized sulphur (-C-SO_x-C-, x = 2, 3).[22, 41, 42]

The Co 2p spectrum (Figures 4 (e)) presented two main peaks at ≈ 780 and 795 eV corresponding to the $2p_{3/2}$ and $2p_{1/2}$ spin-orbital doublets and each of these peaks were deconvoluted into two components. The spectrum was fitted with two couples of peaks with

binding energies at 779.7 and 795.0 eV assigned to Co^{3+} and 781.5 and 796.8 eV assigned to Co^{2+}.[28, 39, 43, 44] Additionally, three small peaks are present at 784.8, 788.9 and 803.3 eV. The first two are ascribed to shake-up satellite peaks of Co $2p_{3/2}$ peak and the third to shake-up satellite peak of the Co $2p_{1/2}$ peak.[43] The existence of Co in two oxidation states validates the suggested spinel structure suggested by the Raman and XRD results. Furthermore, the energy difference between each pair of peaks ($\Delta 2p_{3/2}$-$2p_{1/2}$) was estimated to be 15.3 eV which is in good agreement with the reported values for the mixed valence cobalt oxide Co_3O_4.[28] The Mn 2p spectrum (Figures S4 (e)) also presented two main peaks which were deconvoluted into 2 components each. The spectrum was fitted with two couples of peaks with binding energies at 640.9 and 652.5 eV assigned to Mn^{3+} and 642.5 and 654.1 eV assigned to Mn^{2+}.[17, 29, 45, 46] In addition, a peak at 644.9 eV was observed, which corresponds to the satellite of the Mn $2p_{3/2}$ component. As for the cobalt spectrum, the existence of two components for each Mn 2p peaks indicates that manganese is present in two oxidation states which is consistence with the presence of Mn_3O_4 spinel structure, corroborating the XRD results.

(Insert Figure 4)

The morphology of N_3S_3-GF, Co/N_3S_3-GF and Mn/N_3S_3-GF was assessed by TEM and SEM. Figure 5 shows the TEM micrographs for N_3S_3-GF (a, b), Co/N_3S_3-GF (c, d) and Mn/N_3S_3-GF (e, f) while the corresponding SEM images can be observed in Figure S5. The acquired SEM images for the N_3S_3-GF (Figure S5 (a)) suggest that this doped graphene flakes are composed by wrinkled graphene sheets which is corroborate by TEM images. The TEM micrographs for Co/N_3S_3-GF and Mn/N_3S_3-GF nanocomposites clearly show the presence of Co_3O_4 and Mn_3O_4 nanoparticles agglomerates immobilized onto the N_3S_3-GF surface, respectively. It is also possible to observe the quasi-spherical morphology of the

nanoparticles. Furthermore, a wide size distribution for both nanocomposites is observed with Mn/N_3S_3-GF presenting higher size. These TEM results are corroborated by the SEM analysis were graphene sheets are fully covered by the Co_3O_4 and Mn_3O_4 agglomerates. The EDS analysis (Figure S5 (d, e)) also confirmed the existence of a high content of Co and Mn species.

(Insert Figure 5)

3.2.

3.3.Electrocatalytic performance towards ORR

The ORR electrocatalytic performances of the as-prepared N_3S_3-GF, Co/N_3S_3-GF and Mn/N_3S_3-GF composites were initially evaluated by CV tests in N_2- and O_2-saturated 0.1 mol dm^{-3} KOH electrolyte (catalyst loading of 0.26 mg cm^{-2}). All the CVs of the prepared composites, as well as, those for pristine graphene flakes and Pt/C (20 wt. %) (obtained in N_2- and O_2-saturated KOH) can be observed in Figure S5 (SI). In N_2-saturated electrolyte, no electrochemical processes are observed for GF and N_3S_3-GF, while for Co/N_3S_3-GF and Mn/N_3S_3-GF composites some low intensity peaks can be observed at E_{pc} = 0.78 V and E_{pa} = 1.07 and 1.26 V vs. RHE for Co/N_3S_3-GF and E_{pc} = 0.86 V and E_{pa} = 1.00 V vs. RHE for Mn/N_3S_3-GF. These can be attributed to cobalt and manganese redox processes, respectively.[47-49]

In the presence of O_2, all the prepared materials show an irreversible ORR peak at E_{pc} = 0.76, 0.81 and 0.80 V vs. RHE for N_3S_3-GF, Co/N_3S_3-GF and Mn/N_3S_3-GF, respectively. In the same experimental conditions, Pt/C (20 wt. %) (Figure S5 (b), SI) showed the ORR peak at E_{pc} = 0.88 V vs. RHE.

The ORR electrocatalytic behaviour of the different electrocatalysts was further evaluated by LSV at 1600 rpm in O_2-saturated KOH. As it can be observed in Figure 6 (a),

the Co/N_3S_3-GF and the Mn/N_3S_3-GF composites present very similar diffusion-limiting current density ($j_{L,\ 0.26V,\ 1600rpm}$) values (-3.98 and -4.17 mA cm^{-2}, respectively). The doping of pristine GF with both sulphur and nitrogen also leads to an increase in the j_L values from -3.17 mA cm^{-2} (GF) to -3.49 mA cm^{-2} (N_3S_3-GF). Still, the values obtained are smaller than that obtained for Pt/C (-4.68 mA cm^{-2}). Additionally, both the Co/N_3S_3-GF and Mn/N_3S_3-GF electrocatalysts exhibit similar onset potentials (E_{onset} = 0.87 V) to Pt/C (E_{onset} = 0.91 V vs. RHE). The E_{onset} values of N_3S_3-GF and GF were slightly less positive with E_{onset} = 0.84 and 0.82 V vs. RHE, respectively.

The E_{onset} values obtained for Mn/N_3S_3-GF and Co/N_3S_3-GF nanocomposites are comparable with several reported results for manganese and cobalt oxide nanoparticles immobilized at different carbon materials or even better as it can be observed in Table S2.

To get more information regarding the ORR process, LSVs were acquired at different rotation speeds ranging from 400 to 3000 rpm (Figure S6) and then the kinetic parameters were evaluated using the K-L plots. The K-L plots of GF, Pt/C (20 wt. %) and the three prepared materials (N_3S_3-GF, Co/N_3S_3-GF and Mn/N_3S_3-GF) are presented in Figure S7. All materials present a linear relationship between j^{-1} vs. $\omega^{-1/2}$ suggesting a 1st order O_2 electrocatalytic reduction reaction relatively to the dissolved O_2 concentration. In addition, the K-L plots of Co/N_3S_3-GF, Mn/N_3S_3-GF and Pt/C present parallel lines with very similar slopes between 0.26 and 0.55 V vs. RHE suggesting that the number of electrons transferred per O_2 molecule (n_{O2}) is independent of the potential. This contrasts with what is observed for N_3S_3-GF and pristine GF with the later showing higher differences in the slopes.

The ORR process, in alkaline medium can occur through a direct or an indirect pathway. The first involves 4-electrons, with the direct reduction of O_2 to H_2O/HO^- and the second (indirect) involves a first step where oxygen is reduced to HO_2^- and, a second where the intermediates are reduced to H_2O/HO^- .[6] The n_{O2} values were estimated by the K-L eq.

(see SI), and Fig. 6 (b) shows the plots of n_{O2} vs. *E*. For Pt/C, Co/N_3S_3-GF and Mn/N_3S_3-GF, the n_{O_2} values are practically constant in the range of potentials between 0.26 V and 0.60, vs. RHE, with estimated n_{O_2} values of approximately 4.0, 4.0 and 3.7. For the N_3S_3-GF the n_{O_2} values changed from 4.0 to 3.6 with a mean value of 3.8 while for GF the values decrease from 2.5 to 2.0 with $\tilde{n}_{O_2}$ = 2.2. These results suggest that in the potential range scanned, GF is involved in a 2-electron process, namely, indirect reduction through peroxide pathway while, for the as-prepared materials (N_3S_3-GF, Co/N_3S_3-GF and Mn/N_3S_3-GF) a single step 4-electron transfer mechanism seems to be the leading process.

The results obtained for the prepared dual-doped N_3S_3-GF are similar or even better than those in literature for N, S dual-doped carbon materials.[50-54] For example, Liu et al.[51] reported a S,N-co-doped graphene showing E_{onset} values of 0.88 V, $\tilde{n}_{O_2} \approx 4.0$ and j_L = 5.18 mA cm^{-2} but much higher N content was reported in their ECs (7.25%). The same authors reported sulphur-nitrogen co-doped carbon foam with E_{onset} = 0.80 V and $\tilde{n}_{O_2}$ = 3.96, but as in previous example the ECs presented higher N and S contents (6.53 and 2.88%, respectively).[50] Other examples are the co-doped MWCNT reported by Patil et al.[52] and the co-doped porous carbon sheets by Lu and co-workers.[54]

The better ORR performances (j_L and $\tilde{n}_{O2}$) of N_3S_3-GF, Co/N_3S_3-GF and Mn/N_3S_3-GF when compared to pristine graphene flakes are due to the dual-doping (valid for the 3 nanomaterials) and also to the interactions between the N and S configurations and the Co_3O_4 or Mn_3O_4 nanoparticles. First, the presence of dopants in the carbon matrix usually introduces different charges or spin distribution of the sp^2 carbon plane, which further facilitates the adsorption and activation of O_2 promoting the ORR. Even though, several dopants can be used, N has proven to be the most promising one to improve the ORR activity of carbon-based materials. Pyridinic N atoms, since they possess one lone pair of electrons in addition to the electron donated to the conjugated π bond of graphene, facilitate reductive O_2 adsorption

and therefore have been reported to serve as ORR electrocatalytic sites.[55] Graphitic N is also known to be an active site for ORR.[55, 56] In our case, the slightly better performance of the Co/N_3S_3-GF and Mn/N_3S_3-GF electrocatalysts cannot be directly related to the N% as both present a lower value (1.3 and 1.4%, respectively) compared to N_3S_3-GF (1.7%, Table 1) nor to the percentages of pyridinic or graphitic N atoms (see Table S1). So, this suggests that other factors are influencing the ORR electrocatalytic activity. The simultaneous incorporation of different heteroatoms is also known to improve the ORR activity.[57] The co-existence of different dopants increases spin/charge densities leading to the creation of more active sites and possible interactions between them can improve the activity of single active sites.[58] Also, sulphur is known to have a strong synergistic effect with the nitrogen as the former has a superior radius than those of C and N, promoting charge dislocation, leading to structural defects in the carbon frame, and improving O_2 adsorption. The N_3S_3-GF and Mn/N_3S_3-GF presented the same percentage of S atoms (0.4%) which was very close to the one obtained for Co/N_3S_3-GF (0.3%). However, for the Mn/N_3S_3-GF nanocomposite the amount of oxidized sulphur (-C-SO_x-C-, x = 2, 3) was significantly higher (48.3%) when compared with Co/N_3S_3-GF (28.9%) and N_3S_3-GF (26.6%). The in-situ preparation of the nanoparticles in the presence of N_3S_3-GF leads to changes in the sulphur configuration which may also contribute to the slightly better performance of Co/N_3S_3-GF and Mn/N_3S_3-GF. These results are in good agreement with the work published by Xia and co-workers[59]. They studied the catalytic activity of S-doped graphene by both experimental and density functional theory and concluded that the catalytic e□ciency can be improved through the introduction of $-SO_2-$ bonding structures during the process of doping graphene.[59] Furthermore, the covalent coupling effects between Co_3O_4 and Mn_3O_4 nanoparticles and the S, N co-doped graphene flakes also contribute to Co/N_3S_3-GF and Mn/N_3S_3-GF better performances.

Tafel plots (Figure 6 (c)) were obtained from LSV data in Figure 6 (a) at 1600 rpm, in O_2-saturated KOH. The ORR process exhibits Tafel slopes of 87, 49, 76, 50 and 90 mv dec^{-1} for Pt/C, GF, N_3S_3-GF, Co/N_3S_3-GF and Mn/N_3S_3-GF, respectively. As the estimated Tafel slopes of GF, N_3S_3-GF, Co/N_3S_3-GF are close to 60 mV dec^{-1}, the predicted mechanism where the global reaction rate is ruled by the conversion of MOO^- (intermediate surface adsorbed specie) to MOOH (M is an empty site on the electrocatalyst surface) could probably be ascribed for these materials while for Mn/N_3S_3-GF most likely the rate is determined by the first discharge step or the upon consumption of the MOOH species with high coverage of MOO^-.[60]

(Insert Figure 6)

To confirm the results obtained for N_3S_3-GF, Co/N_3S_3-GF and Mn/N_3S_3-GF, the ORR mechanistic pathway was also explored using the RRDE measurements. The measured current densities during LSV at the electrode disk and ring are shown in Figure 7 (a). The results for Pt/C are also included for comparison. The estimated % H_2O_2 produced was calculated through Eq. 4 and is presented in Figure 7 (b). Both the Co/N_3S_3-GF and Mn/N_3S_3-GF electrocatalysts presented relatively low % H_2O_2 (12% and 14%, respectively) while a value of 4% was obtained for Pt/C. Still, the N_3S_3-GF electrocatalyst presented a H_2O_2 percentage of approximately 26%. Even though these values seem to be in accordance with the $\tilde{n}$ values estimated from the K-L plots, for the Pt/C, Co/N_3S_3-GF and Mn/N_3S_3-GF electrocatalysts, the same does not stand for N_3S_3-GF. The same problem has been reported by several authors.[49, 61-65] According to a recent paper by Qiao *et al.* [65] both methods have limitations and cannot be compared, being this the reason why many authors only present the values obtained by one of the methods. One the one hand, the oxidation of H_2O_2 on Pt is not a mass-transfer limited process. In contrast, and according to the SEM and TEM

results, our catalysts present a rough and porous structure which may change the geometry of the electrode and introduce turbulence in the electrolyte flow leading to estimated *n* values that may not reflect the real catalytic behaviour.

(Insert Figure 7)

Tolerance to methanol crossover was evaluated since in methanol fuel cells this can reduce drastically the cathodic performance, if the EC is sensitive to it. So, the effect of methanol presence was evaluated by chronoamperometry in O_2-saturated KOH (0.1 mol dm^{-3}) to which was added 0.5 mol dm^{-3} methanol at t = 500 s (Figure 8 (a)). For Pt/C, the addition of methanol causes a current decrease to ≈ 52%. The doped graphene (N_3S_3-GF) is also quite sensitive to methanol as it presents a current decrease of 40%. Oppositely, the same material after the immobilization of the cobalt oxide and manganese oxide nanoparticles (Co/N_3S_3-GF and Mn/N_3S_3-GF) are not as sensitive to it as they present current retention between 76 and 81%. This suggests a greater selectivity towards ORR and the good tolerance to methanol crossover effect.

Additionally, an important parameter when evaluating the performance of ORR electrocatalysts is their stability. So, the stability of Co/N_3S_3-GF and Mn/N_3S_3-GF was evaluated by chronoamperometry at E = 0.50 V vs. RHE during 20 000s, in O_2-saturated KOH solution (0.1 mol dm^{-3}) at 1600 rpm. Chronoamperometric responses of these two materials and Pt/C are presented in Figure 8 (b). The commercial Pt/C electrocatalyst presented an 87% current retention after 20 000 s. The Mn/N_3S_3-GF electrocatalyst showed a better result (85%) when compared with Co/N_3S_3-GF (76%) and being very close to Pt/C.

(Insert Figure 8)

4. Conclusions

In this paper, we have reported a simple, scalable and cost-effective method for the synthesis of novel graphene-based nanocomposites, based on the Co_3O_4 or Mn_3O_4 in situ co-precipitation in the presence of dual doped (S, N) graphene flakes, with enhanced properties towards the ORR. The graphene flakes dual doping was achieved using, for the first time, trithiocyanuric acid as the nitrogen and sulphur dopant.

The characterization of both materials, Co/N_3S_3-GF and Mn/N_3S_3-GF, showed the preservation of Co_3O_4 and Mn_3O_4 spinel structure, respectively. Both nanocomposites, as well as the doped GF showed superior overall ORR electrocatalytic activity in alkaline medium with onset potential between 0.84 and 0.87 V vs. RHE, low Tafel slopes (50 – 90 mV dec^{-1}) and good diffusion-limiting current densities (-3.49 – -4.17 mA cm^{-2}). The slightly better performances of Co/N_3S_3-GF and Mn/N_3S_3-GF were attributed to covalent coupling effects between Co_3O_4 and Mn_3O_4 nanoparticles and the N, S dual-doped graphene flakes. Moreover, these electrocatalysts presented good tolerance to methanol poisoning and good stability up to 5.5 hours. This proof of concept study resulted in the development of efficient and stable noble metal-free electrocatalysts with good ORR performance by a simple, cost-effective and scalable method.

Acknowledgments

The authors thank FCT for funding this work through: Project UNIRCELL - POCI-01-0145-FEDER-16422 and project UID/QUI/50006/2013-POCI/01/0145/FEDER/007265.

REFERENCES

[1] P. Chandran, A. Ghosh, S. Ramaprabhu, High-performance Platinum-free oxygen reduction reaction and hydrogen oxidation reaction catalyst in polymer electrolyte membrane fuel cell, Sci Rep, 8 (2018) 11.
[2] Y. Nie, L. Li, Z.D. Wei, Recent advancements in Pt and Pt-free catalysts for oxygen reduction reaction, Chem. Soc. Rev., 44 (2015) 2168-2201.
[3] J. Stacy, Y.N. Regmi, B. Leonard, M.H. Fan, The recent progress and future of oxygen reduction reaction catalysis: A review, Renew. Sust. Energ. Rev., 69 (2017) 401-414.
[4] W. Xia, A. Mahmood, Z.B. Liang, R.Q. Zou, S.J. Guo, Earth-Abundant Nanomaterials for Oxygen Reduction, Angew. Chem.-Int. Edit., 55 (2016) 2650-2676.
[5] R. Cao, J.S. Lee, M.L. Liu, J. Cho, Recent Progress in Non-Precious Catalysts for Metal-Air Batteries, Adv. Energy Mater., 2 (2012) 816-829.
[6] C. Freire, D.M. Fernandes, M. Nunes, V.K. Abdelkader, POM & MOF-based Electrocatalysts for Energy-related Reactions, ChemCatChem, 10 (2018) 1703-1730.
[7] Y.Y. Liang, H.L. Wang, J.G. Zhou, Y.G. Li, J. Wang, T. Regier, H.J. Dai, Covalent Hybrid of Spinel Manganese-Cobalt Oxide and Graphene as Advanced Oxygen Reduction Electrocatalysts, J. Am. Chem. Soc., 134 (2012) 3517-3523.
[8] Z.W. Chen, D. Higgins, A.P. Yu, L. Zhang, J.J. Zhang, A review on non-precious metal electrocatalysts for PEM fuel cells, Energy Environ. Sci., 4 (2011) 3167-3192.
[9] H.Y. Zhu, S. Zhang, Y.X. Huang, L.H. Wu, S.H. Sun, Monodisperse MxFe3-xO4 (M = Fe, Cu, Co, Mn) Nanoparticles and Their Electrocatalysis for Oxygen Reduction Reaction, Nano Lett., 13 (2013) 2947-2951.
[10] Y.J. Sa, K. Kwon, J.Y. Cheon, F. Kleitz, S.H. Joo, Ordered mesoporous Co3O4 spinels as stable, bifunctional, noble metal-free oxygen electrocatalysts, J. Mater. Chem. A, 1 (2013) 9992-10001.
[11] Y.Y. Liang, Y.G. Li, H.L. Wang, J.G. Zhou, J. Wang, T. Regier, H.J. Dai, Co3O4 nanocrystals on graphene as a synergistic catalyst for oxygen reduction reaction, Nat. Mater., 10 (2011) 780-786.
[12] M.P. Araujo, M. Nunes, I.M. Rocha, M.F.R. Pereira, C. Freire, Co3O4 Nanoparticles Anchored on Selectively Oxidized Graphene Flakes as Bifunctional Electrocatalysts for Oxygen Reactions, ChemistrySelect, 3 (2018) 10064-10076.
[13] T.T. Zhang, C.S. He, F.Z. Sun, Y.Q. Ding, M.C. Wang, L. Peng, J.H. Wang, Y.Q. Lin, Co3O4 nanoparticles anchored on nitrogen-doped reduced graphene oxide as a multifunctional catalyst for H2O2 reduction, oxygen reduction and evolution reaction, Sci Rep, 7 (2017) 11.
[14] Y.Y. Liang, H.L. Wang, P. Diao, W. Chang, G.S. Hong, Y.G. Li, M. Gong, L.M. Xie, J.G. Zhou, J. Wang, T.Z. Regier, F. Wei, H.J. Dai, Oxygen Reduction Electrocatalyst Based on Strongly Coupled Cobalt Oxide Nanocrystals and Carbon Nanotubes, J. Am. Chem. Soc., 134 (2012) 15849-15857.
[15] G.J. Zhang, C.X. Li, J. Liu, L. Zhou, R.H. Liu, X. Han, H. Huang, H.L. Hu, Y. Liu, Z.H. Kang, One-step conversion from metal-organic frameworks to Co3O4@N-doped carbon nanocomposites towards highly efficient oxygen reduction catalysts, J. Mater. Chem. A, 2 (2014) 8184-8189.
[16] K. Kumar, I. Abidat, C. Canaff, A. Habrioux, C. Morais, T.W. Napporn, K.B. Kokoh, Metal Loading Effect on the Activity of Co3O4/N-Doped Reduced Graphene Oxide Nanocomposites as Bifunctional Oxygen Reduction/Evolution Catalysts, ChemElectroChem, 5 (2018) 483-493.
[17] J.J. Duan, S. Chen, S. Dai, S.Z. Qiao, Shape Control of Mn 3 O 4 Nanoparticles on Nitrogen- Doped Graphene for Enhanced Oxygen Reduction Activity, Adv. Funct. Mater., 24 (2014) 2072-2078.
[18] X.Z. Gong, G.Z. Liu, Y.S. Li, D.Y.W. Yu, W.Y. Teoh, Functionalized-Graphene Composites: Fabrication and Applications in Sustainable Energy and Environment, Chem. Mat., 28 (2016) 8082-8118.
[19] P. Trogadas, T.F. Fuller, P. Strasser, Carbon as catalyst and support for electrochemical energy conversion, Carbon, 75 (2014) 5-42.
[20] W. Ai, Z.M. Luo, J. Jiang, J.H. Zhu, Z.Z. Du, Z.X. Fan, L.H. Xie, H. Zhang, W. Huang, T. Yu, Nitrogen and Sulfur Codoped Graphene: Multifunctional Electrode Materials for High-Performance Li-Ion Batteries and Oxygen Reduction Reaction, Adv. Mater., 26 (2014) 6186-+.
[21] N. Zhou, N. Wang, Z.X. Wu, L.G. Li, Probing Active Sites on Metal-Free, Nitrogen-Doped Carbons for Oxygen Electroreduction: A Review, Catalysts, 8 (2018) 16.
[22] B. Jarrais, A. Guedes, C. Freire, Heteroatom-Doped Carbon Nanomaterials as Metal-Free Catalysts for the Reduction of 4-Nitrophenol, ChemistrySelect, 3 (2018) 1737-1748.
[23] D.K. Zhao, L.G. Li, L.H. Xie, N. Zhou, S.W. Chen, Sulfur codoping enables efficient oxygen electroreduction on FeCo alloy encapsulated in N-Doped carbon nanotubes, J. Alloy. Compd., 741 (2018) 368-376.
[24] Z.K. Yang, L. Lin, Y.N. Liu, X. Zhou, C.Z. Yuan, A.W. Xu, Supramolecular polymers-derived nonmetal N, S-codoped carbon nanosheets for efficient oxygen reduction reaction, RSC Adv., 6 (2016) 52937-52944.
[25] Z.X. Pei, H.F. Li, Y. Huang, Q. Xue, Y. Huang, M.S. Zhu, Z.F. Wang, C.Y. Zhi, Texturing in situ: N, S-enriched hierarchically porous carbon as a highly active reversible oxygen electrocatalyst, Energy Environ. Sci., 10 (2017) 742-749.

[26] D.M. Fernandes, H.C. Novais, R. Bacsa, P. Serp, B. Bachiller-Baeza, I. Rodriguez-Ramos, A. Guerrero-Ruiz, C. Freire, Polyoxotungstate@Carbon Nanocomposites As Oxygen Reduction Reaction (ORR) Electrocatalysts, Langmuir, 34 (2018) 6376-6387.
[27] N. Muthuswamy, M.E.M. Buan, J.C. Walmsley, M. Ronning, Evaluation of ORR active sites in nitrogen-doped carbon nanofibers by KOH post treatment, Catal. Today, 301 (2018) 11-16.
[28] V.R. Mate, A. Jha, U.D. Joshi, K.R. Patil, M. Shirai, C.V. Rode, Effect of preparation parameters on characterization and activity of Co3O4 catalyst in liquid phase oxidation of lignin model substrates, Appl. Catal. A-Gen., 487 (2014) 130-138.
[29] Z.Y. Tian, P.M. Kouotou, N. Bahlawane, P.H.T. Ngamou, Synthesis of the Catalytically Active Mn3O4 Spinel and Its Thermal Properties, J. Phys. Chem. C, 117 (2013) 6218-6224.
[30] K.H. Wu, Q.C. Zeng, B.S. Zhang, X. Leng, D.S. Su, I.R. Gentle, D.W. Wang, Structural Origin of the Activity in Mn3O4-Graphene Oxide Hybrid Electrocatalysts for the Oxygen Reduction Reaction, ChemSusChem, 8 (2015) 3331-3339.
[31] D.M. Fernandes, M.P. Araujo, A. Haider, A.S. Mougharbel, A.J.S. Fernandes, U. Kortz, C. Freire, Polyoxometalate-graphene Electrocatalysts for the Hydrogen Evolution Reaction, ChemElectroChem, 5 (2018) 273-283.
[32] L. Malavasi, P. Galinetto, M.C. Mozzati, C.B. Azzoni, G. Flor, Raman spectroscopy of AMn(2)O(4) (A = Mn, Mg and Zn) spinels, Phys. Chem. Chem. Phys., 4 (2002) 3876-3880.
[33] L.F. Yang, S. Cheng, X. Ji, Y. Jiang, J. Zhou, M.L. Liu, Investigations into the origin of pseudocapacitive behavior of Mn3O4 electrodes using in operando Raman spectroscopy, J. Mater. Chem. A, 3 (2015) 7338-7344.
[34] D.F. Qiu, G. Bu, B. Zhao, Z.X. Lin, L. Pu, L.J. Pan, Y. Shi, In situ growth of mesoporous Co3O4 nanoparticles on graphene as a high-performance anode material for lithium-ion batteries, Mater. Lett., 119 (2014) 12-15.
[35] S.M. Abbas, S.T. Hussain, S. Ali, N. Ahmad, N. Ali, K.S. Munawar, Synthesis of carbon nanotubes anchored with mesoporous Co3O4 nanoparticles as anode material for lithium-ion batteries, Electrochim. Acta, 105 (2013) 481-488.
[36] T.K. Mondal, D. Dinda, S.K. Saha, Nitrogen, sulphur co-doped graphene quantum dot: An excellent sensor for nitroexplosives, Sens. Actuator B-Chem., 257 (2018) 586-593.
[37] M.E. Lipinska, S.L.H. Rebelo, M.F.R. Pereira, J. Gomes, C. Freire, J.L. Figueiredo, New insights into the functionalization of multi-walled carbon nanotubes with aniline derivatives, Carbon, 50 (2012) 3280-3294.
[38] M.P. Araujo, O. Soares, A.J.S. Fernandes, M.F.R. Pereira, C. Freire, Tuning the surface chemistry of graphene flakes: new strategies for selective oxidation, RSC Adv., 7 (2017) 14290-14301.
[39] T. Warang, N. Patel, R. Fernandes, N. Bazzanella, A. Miotello, Co3O4 nanoparticles assembled coatings synthesized by different techniques for photo-degradation of methylene blue dye, Appl. Catal. B-Environ., 132 (2013) 204-211.
[40] Z.H. Sheng, L. Shao, J.J. Chen, W.J. Bao, F.B. Wang, X.H. Xia, Catalyst-Free Synthesis of Nitrogen-Doped Graphene via Thermal Annealing Graphite Oxide with Melamine and Its Excellent Electrocatalysis, ACS Nano, 5 (2011) 4350-4358.
[41] Y. Liu, Y. Qiao, G.Y. Wei, S. Li, Z.S. Lu, X.B. Wang, X.D. Lou, Sodium storage mechanism of N, S co-doped nanoporous carbon: Experimental design and theoretical evaluation, Energy Storage Mater., 11 (2018) 274-281.
[42] Y.P. Guo, Z.Q. Zeng, Y.L. Li, Z.G. Huang, Y. Cui, In-situ sulfur-doped carbon as a metal-free catalyst for persulfate activated oxidation of aqueous organics, Catal. Today, 307 (2018) 12-19.
[43] T.Y. Ma, S. Dai, M. Jaroniec, S.Z. Qiao, Metal-Organic Framework Derived Hybrid Co3O4-Carbon Porous Nanowire Arrays as Reversible Oxygen Evolution Electrodes, J. Am. Chem. Soc., 136 (2014) 13925-13931.
[44] S.P. Mo, S.D. Li, J.Q. Li, Y.Z. Deng, S.P. Peng, J.Y. Chen, Y.F. Chen, Rich surface Co(III) ions-enhanced Co nanocatalyst benzene/toluene oxidation performance derived from (CoCoIII)-Co-II layered double hydroxide, Nanoscale, 8 (2016) 15763-15773.
[45] F. Gao, J.Y. Qu, Z.B. Zhao, Q. Zhou, B.B. Li, J.S. Qiu, A green strategy for the synthesis of graphene supported Mn3O4 nanocomposites from graphitized coal and their supercapacitor application, Carbon, 80 (2014) 640-650.
[46] A. Ramirez, P. Hillebrand, D. Stellmach, M.M. May, P. Bogdanoff, S. Fiechter, Evaluation of MnOx, Mn2O3, and Mn3O4 Electrodeposited Films for the Oxygen Evolution Reaction of Water, J. Phys. Chem. C, 118 (2014) 14073-14081.
[47] A. Bergmann, E. Martinez-Moreno, D. Teschner, P. Chernev, M. Gliech, J.F. de Araujo, T. Reier, H. Dau, P. Strasser, Reversible amorphization and the catalytically active state of crystalline Co3O4 during oxygen evolution, Nat. Commun., 6 (2015) 9.
[48] A.J. Carrillo, D.P. Serrano, P. Pizarro, J.M. Coronado, Improving the Thermochemical Energy Storage Performance of the Mn2O3/Mn3O4 Redox Couple by the Incorporation of Iron, ChemSusChem, 8 (2015) 1947-1954.

[49] J.J. Duan, Y. Zheng, S. Chen, Y.H. Tang, M. Jaroniec, S.Z. Qiao, Mesoporous hybrid material composed of Mn3O4 nanoparticles on nitrogen-doped graphene for highly efficient oxygen reduction reaction, Chem. Commun., 49 (2013) 7705-7707.
[50] Z. Liu, H.G. Nie, Z. Yang, J. Zhang, Z.P. Jin, Y.Q. Lu, Z.B. Xiao, S.M. Huang, Sulfur-nitrogen co-doped three-dimensional carbon foams with hierarchical pore structures as efficient metal-free electrocatalysts for oxygen reduction reactions, Nanoscale, 5 (2013) 3283-3288.
[51] F. Liu, F.S. Niu, T. Chen, J.R. Han, Z. Liu, W.R. Yang, Y.H. Xu, J.Q. Liu, One-step electrochemical strategy for in-situ synthesis of S, N-codoped graphene as metal-free catalyst for oxygen reduction reaction, Carbon, 134 (2018) 316-325.
[52] I.M. Patil, V. Reddy, M. Lokanathan, B. Kakade, Nitrogen and sulphur co-doped multiwalled carbon nanotubes as an efficient electrocatalyst for improved oxygen electroreduction, Appl. Surf. Sci., 449 (2018) 697-704.
[53] A.K. Samantara, S.C. Sahu, A. Ghosh, B.K. Jena, Sandwiched graphene with nitrogen, sulphur co-doped CQDs: an efficient metal-free material for energy storage and conversion applications, J. Mater. Chem. A, 3 (2015) 16961-16970.
[54] C. Yang, H.L. Jin, C.X. Cui, J. Li, J.C. Wang, K. Amine, J. Lu, S. Wang, Nitrogen and sulfur co-doped porous carbon sheets for energy storage and pH-universal oxygen reduction reaction, Nano Energy, 54 (2018) 192-199.
[55] N.P. Subramanian, X.G. Li, V. Nallathambi, S.P. Kumaraguru, H. Colon-Mercado, G. Wu, J.W. Lee, B.N. Popov, Nitrogen-modified carbon-based catalysts for oxygen reduction reaction in polymer electrolyte membrane fuel cells, J. Power Sources, 188 (2009) 38-44.
[56] R. O'Hayre, S. Cha, W. Colella, F. Prinz, Fuel Cell Fundamentals, John Wiley & Sons, New York, 2005.
[57] B.B. Huang, Y.C. Liu, X. Huang, Z.L. Xie, Multiple heteroatom-doped few-layer carbons for the electrochemical oxygen reduction reaction, J. Mater. Chem. A, 6 (2018) 22277-22286.
[58] S.S. Shinde, C.H. Lee, A. Sami, D.H. Kim, S.U. Lee, J.H. Lee, Scalable 3-D Carbon Nitride Sponge as an Efficient Metal-Free Bifunctional Oxygen Electrocatalyst for Rechargeable Zn-Air Batteries, ACS Nano, 11 (2017) 347-357.
[59] L.P. Zhang, J.B. Niu, M.T. Li, Z.H. Xia, Catalytic Mechanisms of Sulfur-Doped Graphene as Efficient Oxygen Reduction Reaction Catalysts for Fuel Cells, J. Phys. Chem. C, 118 (2014) 3545-3553.
[60] T. Shinagawa, A.T. Garcia-Esparza, K. Takanabe, Insight on Tafel slopes from a microkinetic analysis of aqueous electrocatalysis for energy conversion, Sci Rep, 5 (2015) 21.
[61] M. Mamlouk, S.M.S. Kumar, P. Gouerec, K. Scott, Electrochemical and fuel cell evaluation of Co based catalyst for oxygen reduction in anion exchange polymer membrane fuel cells, J. Power Sources, 196 (2011) 7594-7600.
[62] Y. Zheng, Y. Jiao, L. Ge, M. Jaroniec, S.Z. Qiao, Two-Step Boron and Nitrogen Doping in Graphene for Enhanced Synergistic Catalysis, Angew. Chem.-Int. Edit., 52 (2013) 3110-3116.
[63] R.F. Zhou, Y. Zheng, D. Hulicova-Jurcakova, S.Z. Qiao, Enhanced electrochemical catalytic activity by copper oxide grown on nitrogen-doped reduced graphene oxide, J. Mater. Chem. A, 1 (2013) 13179-13185.
[64] R.F. Zhou, S.Z. Qiao, Silver/Nitrogen-Doped Graphene Interaction and Its Effect on Electrocatalytic Oxygen Reduction, Chem. Mat., 26 (2014) 5868-5873.
[65] R.F. Zhou, Y. Zheng, M. Jaroniec, S.Z. Qiao, Determination of the Electron Transfer Number for the Oxygen Reduction Reaction: From Theory to Experiment, ACS Catal., 6 (2016) 4720-4728.

FIGURE 1

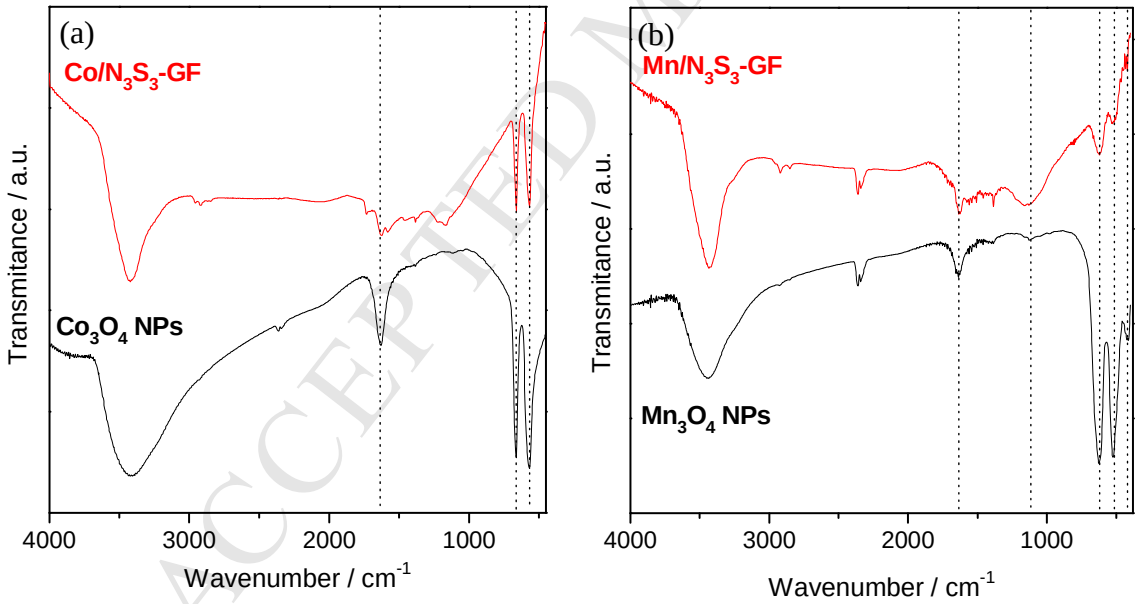

FIGURE 2

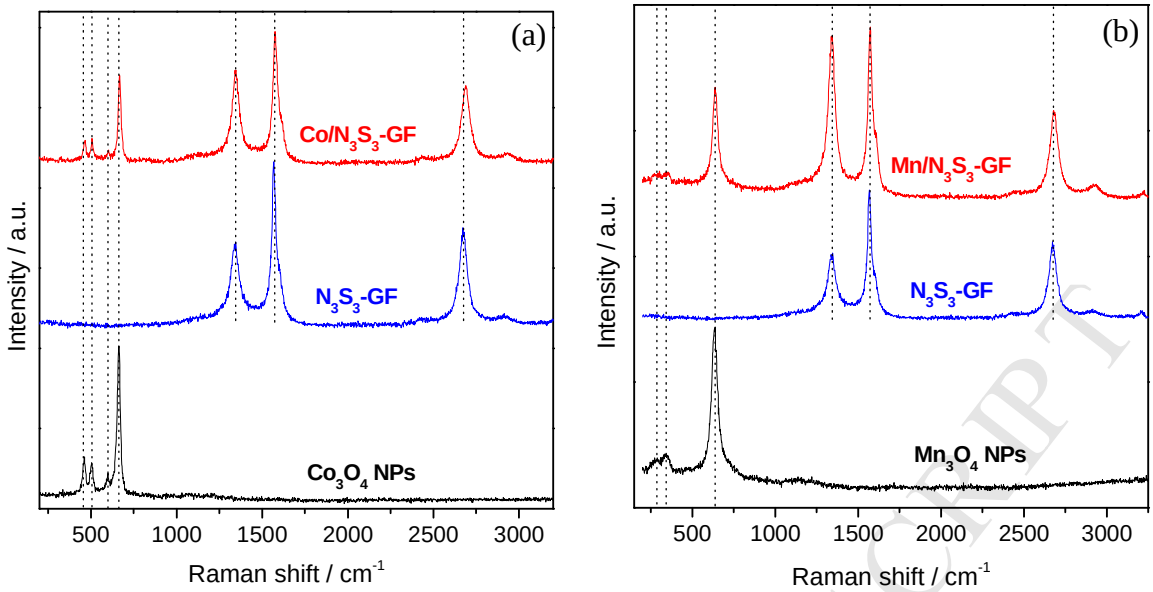

FIGURE 3

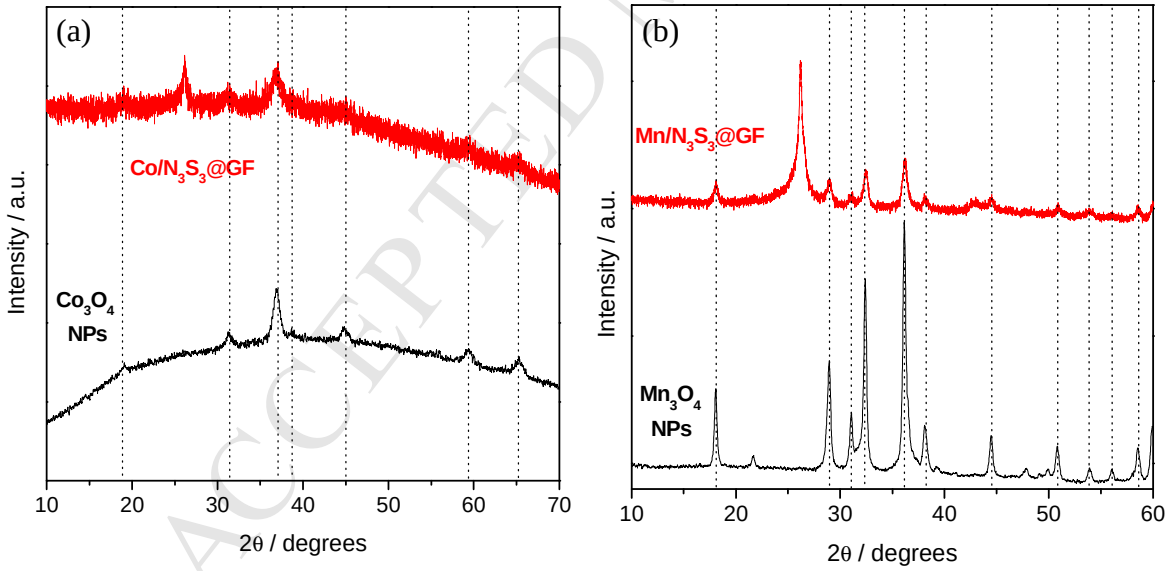

FIGURE 4

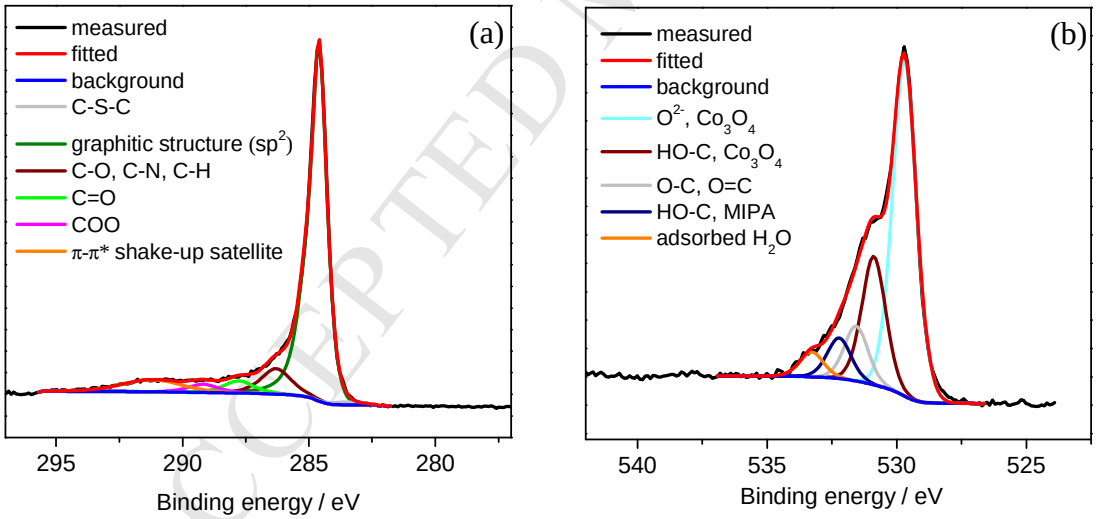

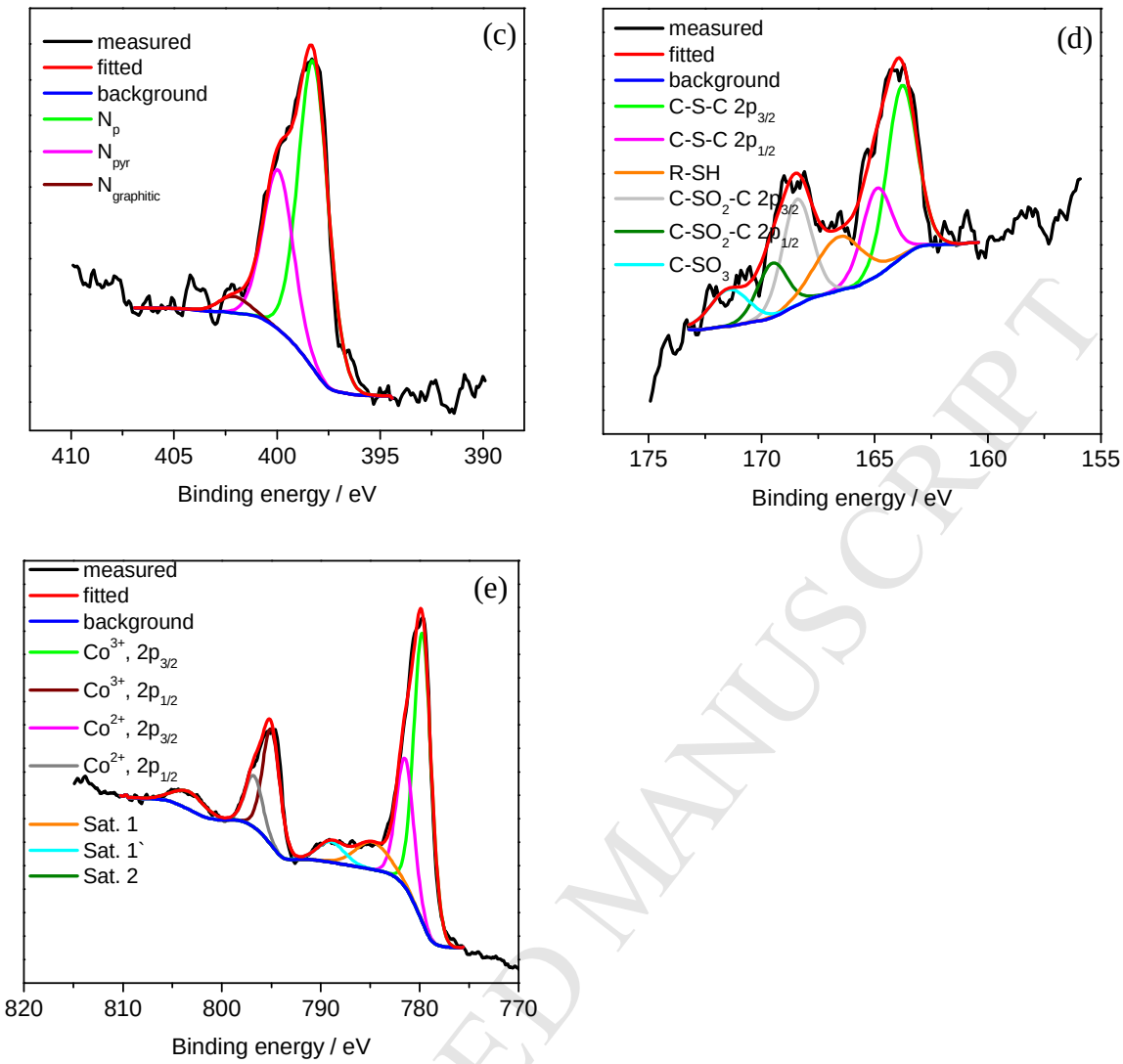
(c)
measured
fitted
background
N_p
N_{pyr}
$N_{graphitic}$
410
405
400
395
390
Binding energy / eV
(d)
measured
fitted
background
C-S-C $2p_{3/2}$
C-S-C $2p_{1/2}$
R-SH
C-SO_2-C $2p_{3/2}$
C-SO_2-C $2p_{1/2}$
C-SO_3
175
170
165
160
155
Binding energy / eV
(e)
measured
fitted
background
Co^{3+}, $2p_{3/2}$
Co^{3+}, $2p_{1/2}$
Co^{2+}, $2p_{3/2}$
Co^{2+}, $2p_{1/2}$
Sat. 1
Sat. 1`
Sat. 2
820
810
800
790
780
770
Binding energy / eV

FIGURE 5

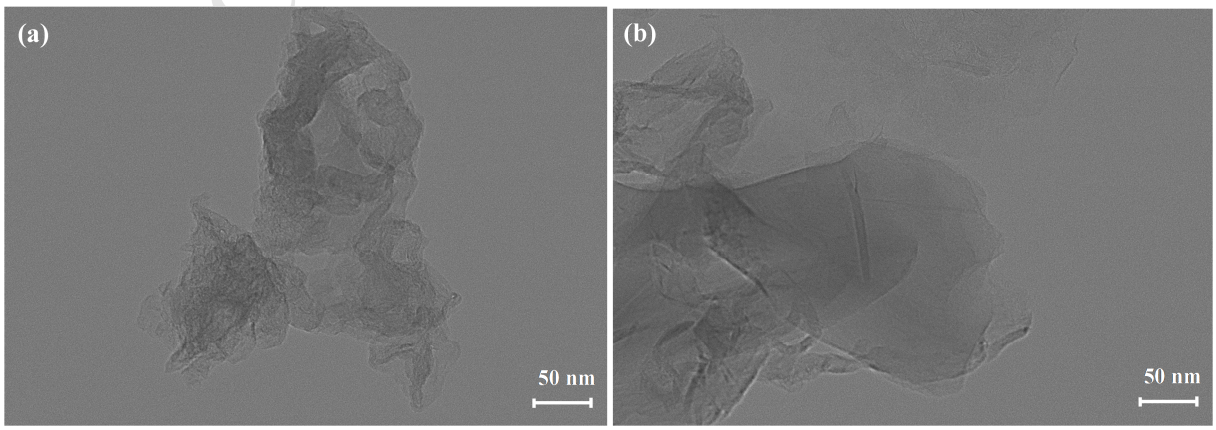
(a)
50 nm
(b)
50 nm

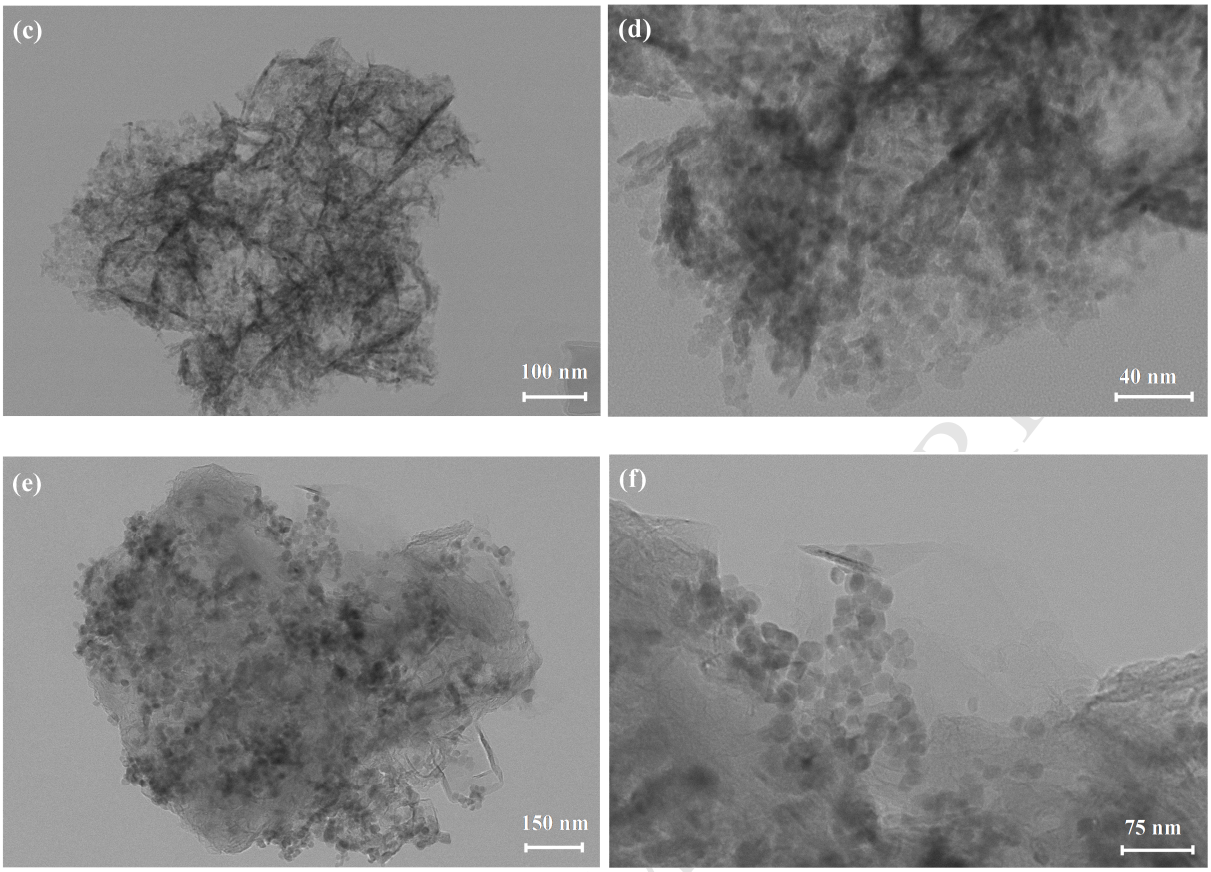

FIGURE 6

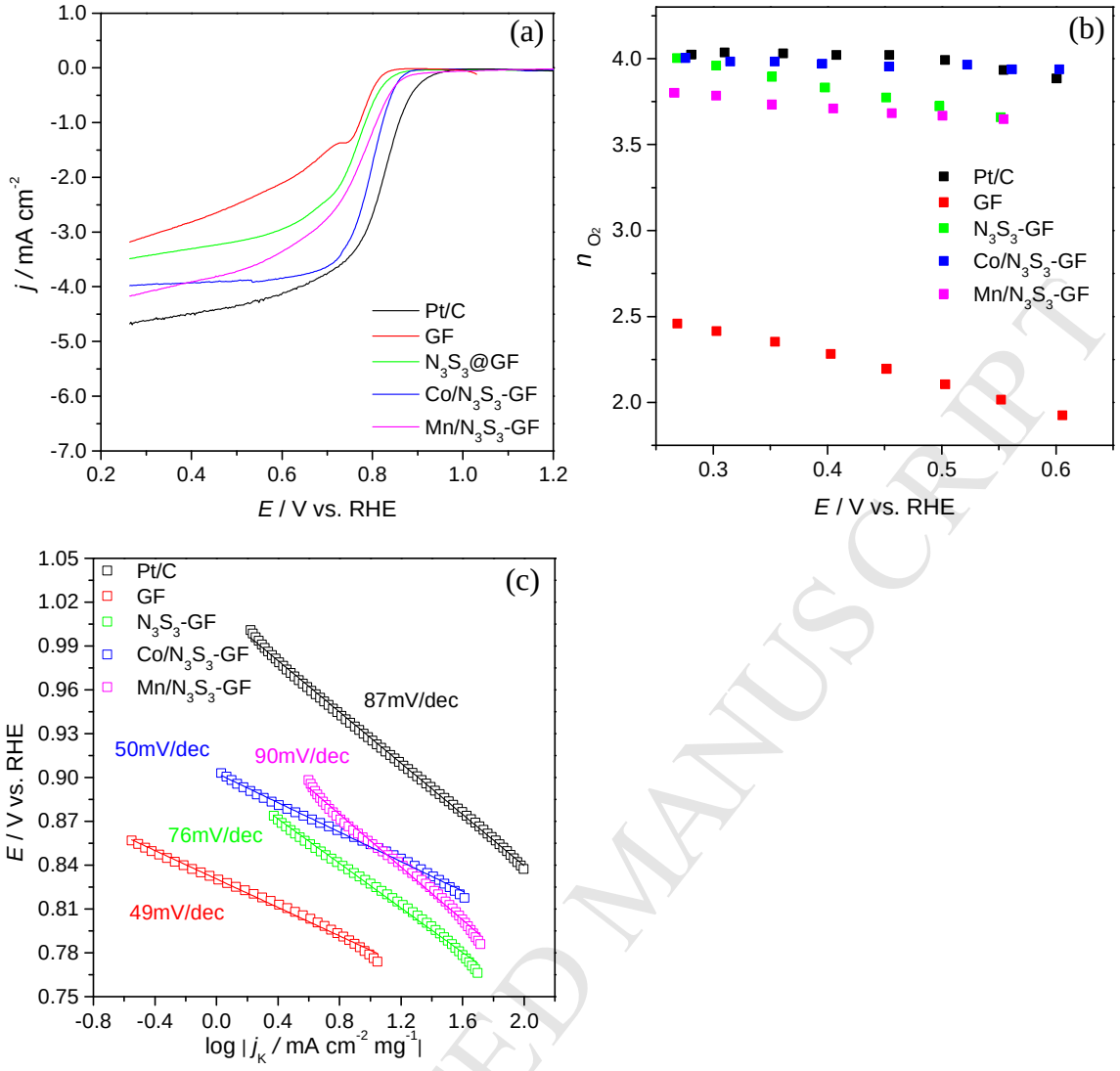

FIGURE 7

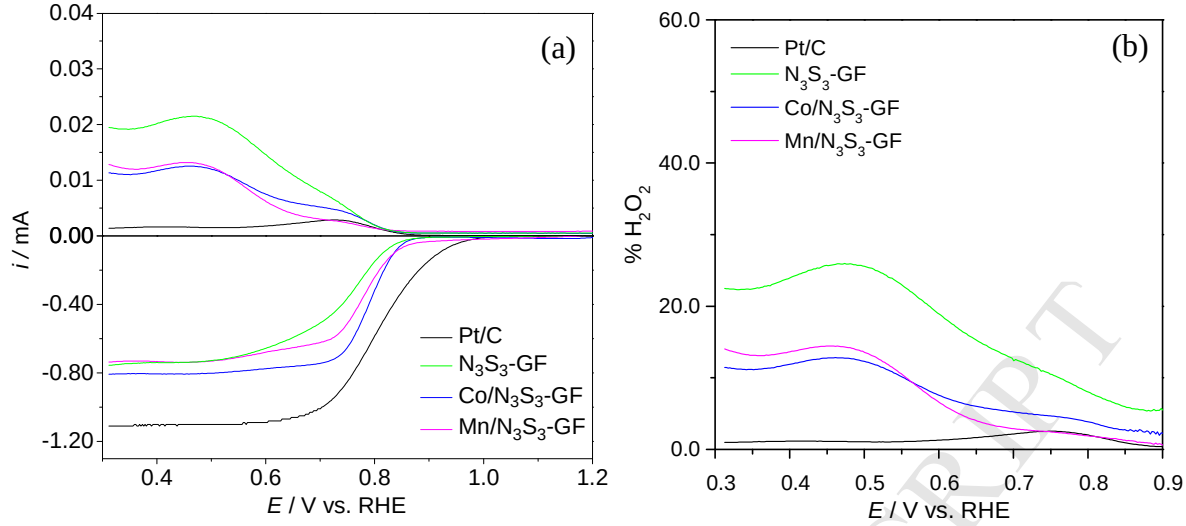

FIGURE 8

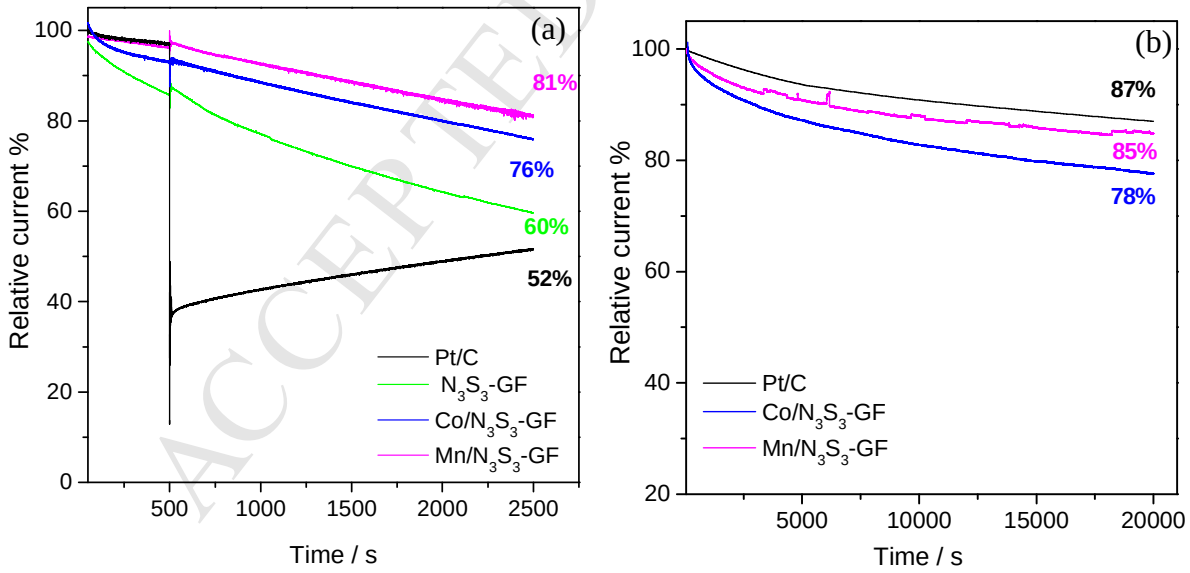

FIGURE CAPTIONS

Figure 1. FTIR spectra of: (a) Co_3O_4 NPs (black) and Co/N_3S_3-GF (red) and (b) Mn_3O_4 NPs (black) and Mn/N_3S_3-GF (red), in the range 4000 – 500 cm^{-1}.

Figure 2. Raman spectra of: (a) Co_3O_4 NPs (black), N_3S_3-GF (blue) and Co/N_3S_3-GF (red) and (b) Mn_3O_4 NPs (black), N_3S_3-GF (blue) and Mn/N_3S_3-GF (red).

Figure 3. XRD spectra of: (a) Co_3O_4 NPs (black) and Co/N_3S_3-GF (red) and (b) Mn_3O_4 NPs (black) and Mn/N_3S_3-GF (red).

Figure 4. Deconvoluted high resolution XPS spectra of Co/N_3S_3-GF: C 1s (a), O 1s (b), N 1s (c), S 2p (d) and Co 2p (e).

Figure 5. TEM micrographs of N_3S_3-GF (a), Co/N_3S_3-GF (b) and Mn/N_3S_3-GF (c).

Figure 6. ORR LSV curves of Pt/C, GF, N_3S_3-GF, Co/N_3S_3-GF and Mn/N_3S_3-GF acquired in O_2-saturated KOH solution (0.1 mol dm^{-3}) at 1600 rpm and 0.005 V s^{-1} (a); n_{O2} at several potential values (b) and the respective ORR Tafel plots (c).

Figure 7. LSVs recorded with RRDE in O_2-saturated 0.1 mol dm^{-3} KOH solution, at 1600 rpm and v = 0.005 V s^{-1} and the ring potential was kept at E = 1.16 V vs. RHE (a); Estimated percentage of H_2O_2 formed (b).

Figure 8. Chronoamperometric responses of the ECs with the addition of 0.5 mol dm^{-3} methanol after ≈ 500 s, at E = 0.50 V vs. RHE, at 1600 rpm, in 0.1 mol dm^{-3} O_2-saturated KOH (a); Chronoamperometric responses of the ECs at E = 0.50 V vs. RHE, at 1600 rpm, in 0.1 mol dm^{-3} O_2-saturated KOH for 20000 s (b).

TABLES

Table 1. XPS surface atomic percentages for GF, N_3S_3-GF, Co/N_3S_3-GF and Mn/N_3S_3-GF[a].

Sample	Atomic %					
	C 1s	**O 1s**	**N 1s**	**S 2p**	**Co 2p**	**Mn 2p**
GF	97.1	2.9	-	-	-	-
N_3S_3-GF	93.7	4.3	1.7	0.4	-	-
Co/N_3S_3-GF	75.3	14.9	1.3	0.3	8.1	-
Mn/N_3S_3-GF	83.6	9.8	1.4	0.4	-	4.7

[a] Determined by the areas of the respective bands in the high-resolution XPS spectra.

Highlights

- N,S dual-doped graphene was successfully prepared by scalable ball-milling method
- Co/N_3S_3-GF and Mn/N_3S_3-GF electrocatalysts showed excellent ORR performance;
- Good stability/durability and tolerance to methanol crossover were achieved.